Energy Technology
Generation, Conversion, Storage, Distribution

Accepted Article

Title: Rational design of manganese cobalt phosphide with yolk-shell structure for overall water splitting

Authors: Guisheng Tang, Ye Zeng, Binbin Wei, Hanfeng Liang, Jian Wu, Pengcheng Yao, and Zhoucheng Wang

To be cited as: *Energy Technol.* 10.1002/ente.201900066

Link to VoR: http://dx.doi.org/10.1002/ente.201900066

www.entechnol.de

WILEY-VCH

WILEY-VCH

Rational design of manganese cobalt phosphide with yolk-shell structure for overall water splitting

Guisheng Tang, Ye Zeng, Binbin Wei, Hanfeng Liang, Jian Wu, Pengcheng Yao, Zhoucheng Wang**

G. S. Tang, Y. Zeng, B. B. Wei, Dr. H. F. Liang, J. Wu, P. C. Yao, Prof. Z. C. Wang
College of Chemistry and Chemical Engineering, Xiamen University, Xiamen 361005, China
E-mail: hanfeng.liang@kaust.edu.sa; zcwang@xmu.edu.cn

Keywords: Mn-Co phosphide, yolk-shell structure, bifunctional catalyst, electrochemistry, overall water splitting

Abstract: The development of low cost, earth-abundant and efficient catalysts for overall water splitting, involving hydrogen evolution reaction (HER) and oxygen evolution reaction (OER), attracts tremendous attention in recent years. Herein, this work reports the preparation of Mn-Co phosphide (Mn-Co-P) bifunctional catalysts with a yolk-shell structure by a facile hydrothermal route. The as-prepared catalysts exhibit excellent catalytic activity with low overpotentials of 66 mV at 10 mA cm^{-2} for HER and 355 mV at 50 mA cm^{-2} for OER in 1 M KOH, along with outstanding stability. More importantly, the cell voltage of 1.74 V can achieve the current density of 10 mA cm^{-2} when assembled as an electrolyzer for overall water splitting. Such superior performance makes the Mn-Co-P being a promising candidate to replace Pt-based noble metal catalysts for electrocatalytic applications.

1. Introduction

The excessive usage of fossil fuels results in inevitably energy crisis and environmental pollution.[1] Nowadays, searching for clean and renewable energy has been urgent.[2-4] With the merits of cleanliness and reproducibility, hydrogen energy has been proposed as a promising alternative to fossil fuels.[5-7] Currently, electrocatalytic water splitting is considered as a facile and efficient way to produce hydrogen.[8] However, the slow kinetics of two half reactions (HER and OER) restrict the efficiency of overall water splitting.[9-12] Precious metal-containing compounds, such as Pt and IrO_2/RuO_2, are the state-of-the-art catalysts for HER and OER, respectively.[13-15] However, their high cost and scarcity severely

limit their practical application.[16-22] Hence, developing low-cost, earth-abundant and efficient non-noble metal catalysts for both HER and OER in alkaline media is urgent yet challenging.[16,23-27]

Transition metal phosphides have emerged as the highly active catalysts for HER due to similar structure of hydrogenase and high durability.[28,29] Moreover, transition metal phosphides also have been confirmed to have good OER activity recently.[30,31] Jiao et al. reported that CoP/rGO displayed excellent catalytic activity towards overall water splitting in alkaline solution.[32] Song et al. demonstrated that $Cu_{0.3}Co_{2.7}P$/NC exhibited prominent OER and HER activity with small overpotentials.[33] Furthermore, compared with binary transition metal phosphides, ternary materials exhibit better catalytic activity and afford lower overpotential.[34] With the consideration of these, we have synthesized the yolk-shell structured Mn-Co-P bifunctional catalysts by a facile method for overall water splitting applications. As a novel material, this core-shell structure has been widely used in electronic and catalytic fields owing to high specific surface area and favorable surface activity.[35] However, the rational design of yolk-shell structures as efficient bifunctional catalysts has rarely been reported.[28] More importantly, the as-prepared Mn-Co-P yolk-shell catalysts exhibit satisfactory performance toward HER and OER, as well as good stability in 1 M KOH.

2. Results and discussion

2.1. Structural characterization

The synthesis of Mn-Co-P is illustrated in **Scheme S1**. The Mn-Co precursor was prepared by hydrothermal method (**Figure S1**). Then, the Mn-Co-P product was obtained by the thermal phosphidation of as-prepared Mn-Co precursor. As we can see from **Figure 1a**, all the diffraction peaks are indexed to the phases of MnCoP (JCPDS no. 41-0809) and CoP (JCPDS no. 29-0497), respectively.[36] XPS was further measured to study the chemical states of the yolk-shell structured Mn-Co-P. For Mn 2p spectrum **(Figure 1b)**, a spin-orbit doublet of Mn $2p_{1/2}$ and Mn $2p_{3/2}$ located at 654.1 and 641.8 eV can be fitted into both Mn^{2+} and Mn^{3+}

while the peak with binding energy of 645.7 eV is indexed to satellite peak (indicated as ñsat.ò).[26,37] In the spectrum of Co 2p **(Figure 1c)**, two satellite peaks close to two spin-orbit doublets at 796.5 and 781 eV correspond to the Co $2p_{1/2}$ and Co $2p_{3/2}$,[26,38] respectively. In detail, the peaks positioned at 780.8 and 796.4 eV show the existence of Co^{3+} while the peaks at 782.9 eV and 799 eV are typically ascribed to Co^{2+}. In the P 2p spectrum **(Figure 1d)**, the peak at 130.4 eV is assigned to metal phosphides, the peak at 133.5 eV is originated from the oxidized P species.[39]

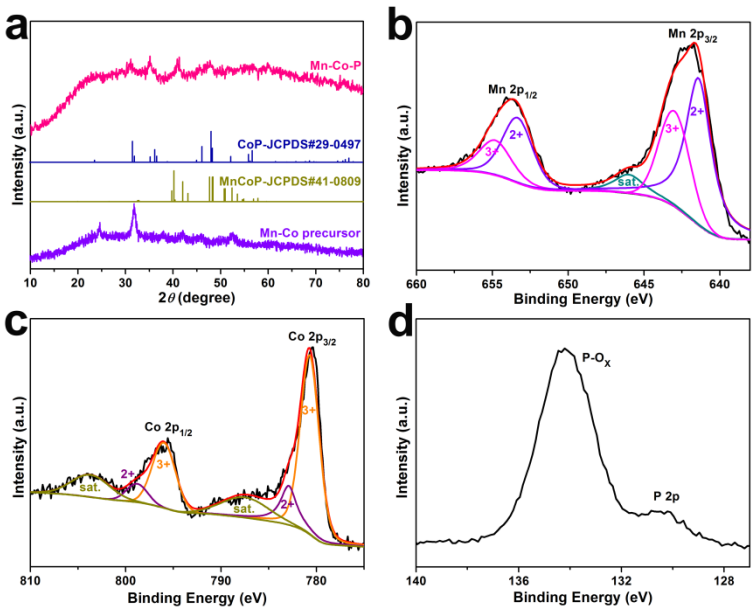

Figure 1. (a) XRD patterns of Mn-Co precursor and Mn-Co-P. (b) Mn 2p, (c) Co 2p, and (d) P 2p XPS spectra of Mn-Co-P.

The scanning electron microscopy (SEM) and high-resolution transmission electron microscopy (HRTEM) were employed to observe the morphologies of the as-synthesized Mn-Co-P samples. As shown in **Figure 2a and 2b**, Mn-Co-P is composed of yolk-shell structured spheres with size of about 5 εm in diameter. Energy dispersive spectrometer (EDS) spectrum supports that yolk and shell share identical elemental composition **(Figure S2)**. Additionally, elemental mapping analysis confirms uniform distribution of Mn, Co and P elements **(Figure 2c)**. The influence of reaction temperatures on the morphologies and phase composition of Mn-Co-P spheres was further studied **(Figure S3, S4 and S5)**. It is noted that there are no

significant differences in phase composition for Mn-Co-P calcined at different temperatures. However, the samples synthesized at 350 ℃ compose of broken spheres whereas the one synthesized at high temperature (450 ℃) tend to aggregate, suggesting that 400 ℃ is the optimal calcination temperature in our system. From HRTEM **(Figure 2d)**, the lattice spacings of 0.224 and 0.283 nm correspond to the (112) plane of MnCoP and the (011) plane of CoP, respectively, further demonstrating the successful preparation of Mn-Co-P spheres with yolk-shell structure.

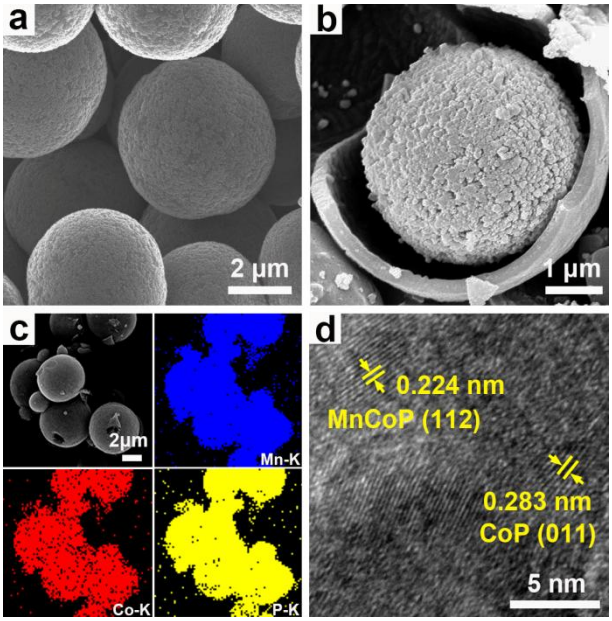

Figure 2. (a,b) SEM, (c) Elemental mapping and (d) High-resolution TEM images of the Mn-Co-P spheres.

2.2. Electrocatalytic performance toward HER

To investigate the HER performance of Mn-Co precursor and Mn-Co-P, linear sweep voltammetry (LSV) curves are tested at a scan rate of 5 mV s^{-1}. Owing to the optimal phosphidation temperature, the Mn-Co-P catalysts obtained at 400 ℃ show the best catalytic performance, in accordance with SEM observations **(Figure S6).** As shown in **Figure 3a**, the Mn-Co-P catalysts exhibit excellent catalytic activity with a small overpotential of 66 mV at 10 mA cm^{-2}, which is lower than Mn-Co precursor (294 mV). Furthermore, this performance is also comparable to or even better than that of other recently reported catalysts **(Table S1)**,

such as CoP NW/Hb (113mV at 10 mA cm^{-2}), CoP/CC (115 mV at 1 mA cm^{-2}) and CoS_2 NA/Ti (140 mV at 10 mA cm^{-2}).[17,23,22] The electrocatalytic kinetics of Mn-Co precursor and Mn-Co-P are evaluated using Tafel plots where the Tafel slope of Mn-Co-P (82 mV dec^{-1}) is much smaller than that of Mn-Co precursor (157 mV dec^{-1}), indicating a fast HER kinetics **(Figure 3b)**. To estimate the electrochemically active surface area (ECSA) and understand the contribution of active site to HER performance, we further evaluate the double layer capacitances (C_{dl}) by a simple cyclic voltammetry method **(Figure 3c**, **S7a** and **S7c)**. Clearly, the Mn-Co-P has a much higher C_{dl} (60.1 mF cm^{-2}) than that of Mn-Co precursor (14.5 mF cm^{-2}), thus resulting in a significant improved catalytic activity. Moreover, the normalized polarization curves **(Figure S8)** suggest the superior intrinsic activity of Mn-Co-P, which could be due to enhanced electrical conductivity **(Figure S9)**. Besides, the Mn-Co-P catalysts display 91% of its initial activity retention after 24 h continuous operation at 10 mA cm^{-2} **(Figure 3d)**. In addition, the polarization curves in **Figure S10a** show slight deviation compared with the initial one after 5000 cycles, again suggesting excellent durability toward HER. We further perform the post-cycled SEM **(Figure S11a)**, TEM **(Figure S12a),** XRD **(Figure S13)** and XPS **(Figure S14a-c)** characterizations, where no significant changes are found after HER.

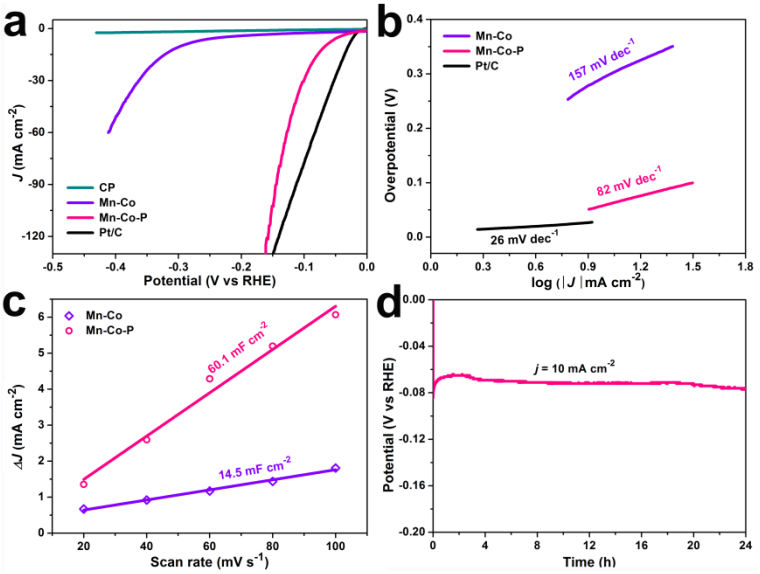

Figure 3. Electrochemical HER activity of Mn-Co-P and Mn-Co precursor: (a) iR-corrected polarization curves (b) Corresponding Tafel plots, (c) Scan rate dependence on current density difference and (d) Chronopotentiometric curve at a constant current density of 10 mA cm^{-2} for 24 h.

2.3. Electrocatalytic performance toward OER

The OER electrocatalytic performance of as-prepared Mn-Co-P and Mn-Co precursor was also investigated. The similar result was obtained where the Mn-Co-P catalysts prepared at 400 ℃ displayed the superior OER performance **(Figure S15)**. From **Figure 4a**, it can be found that the Mn-Co-P catalysts require a much lower overpotential of 355 mV to deliver the current density of 50 mA cm^{-2} compared to Mn-Co precursor (523 mV), which is also superior to that of commercial RuO_2 (380 mV at 50 mV cm^{-2}), CoP NR/C (320 mV at 10 mA cm^{-2}), and NiCo LDH (367 mV at 40 mA cm^{-2}) (see **Table S2** for details).[40,41] The Tafel slopes of Mn-Co-P, RuO_2 and Mn-Co precursor are 58, 88 and 191mV dec^{-1}, respectively **(Figure 4b)**, suggesting that the Mn-Co-P catalysts have the fastest OER kinetics. **Figure 4c** compares the C_{dl} calculated from **Figure S7b** and **S7d** of Mn-Co precursor and Mn-Co-P. In good agreement with better OER activity, the Mn-Co-P catalysts show a larger C_{dl} (14.6 mF cm^{-2}), nearly 1.5 times as that of Mn-Co precursor (9.9 mF cm^{-2}), indicating a higher surface active area and more exposed active sites. Moreover, the Mn-Co-P electrode shows a negligible decrease at 10 mA cm^{-2} after 24 h continuous operation **(Figure 4d)**. And the polarization curve, morphology and structure after 5000 cycles shows no significant change **(Figure S10b, S11b**, **S12b and S13)**, implying the outstanding stability. The XPS characterizations of post-cycled catalysts clearly suggest that Mn^{2+} and Co^{2+} were oxidized to Mn^{3+} and Co^{3+} **(Figure S14d-f)**, showing the formation of metal oxides that are the real active species for OER on the surface.[42]

WILEY-VCH

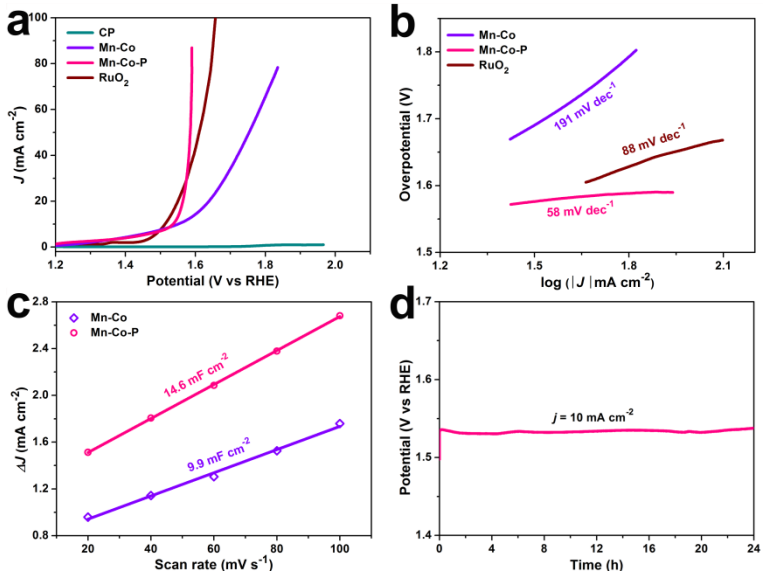

Figure 4. Electrochemical OER activity of Mn-Co-P and Mn-Co precursor: (a) iR-corrected polarization curves, (b) Corresponding Tafel plots, (c) Estimated values of double layer capacitance and (d) Chronopotentiometric curve at a constant current density of 10 mA cm^{-2} for 24 h.

2.4. Overall electrochemical water splitting

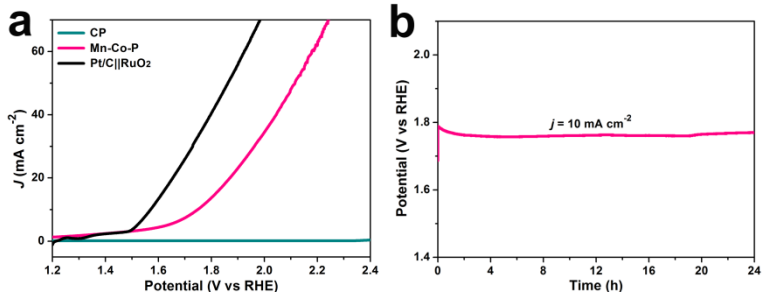

Figure 5. (a) Polarization curves and (b) Chronopotentiometric curve at 10 mA cm^{-2} for 24 h of Mn-Co-P||Mn-Co-P electrolyzer for overall water splitting.

Encouraged by the impressive performance of Mn-Co-P catalysts toward both HER and OER, we further investigate the activity of overall water splitting by using Mn-Co-P as both the cathode and anode. As presented in **Figure 5a**, this Mn-Co-P pair affords the current density of 10 mA cm^{-2} at the voltages of 1.74 V. Although this value is a little higher than that of Pt/C||RuO_2 (1.55 V), it also compares to some materials reported, such as Mn-Co

LDH/graphene (~1.7 V at 10 mA cm^{-2}), $Cu_{0.3}Co_{2.7}P$/NC (1.74 V at 10 mA cm^{-2}) and $Co@Co_3O_4$-NC (2 V at 10 mA cm^{-2}) (also see **Table S3**).[33,43,44] The durability test indicates that the current density barely changes even after 24 h, indicating that the Mn-Co-P||Mn-Co-P electrolyzer possesses exceptional stability toward overall water splitting **(Figure 5b)**. Such superior electrocatalytic activity can be attributed to the following aspects: (1) Unique yolk-shell structure not only increases the effective contact area between catalyst and electrolyte and enables more active sites to be exposed, but also facilitates the charge transfer, thus promoting the electrocatalytic performance;[30,45] (2) The buffer between yolk and shell avoids structural collapse during electrocatalysis process;[46] (3) The synergistic effect of Mn and Co improves the catalytic activity and stability.[16] The presence of Mn in close proximity to Co could lower the activation barrier needed for the formation of intermediates whereas the presence of Co might also improve the stability of Mn.[47]

3. Conclusion

In this work, we have synthesized the yolk-shell structured Mn-Co-P bifunctional catalysts for water splitting electrocatalysis. Owing to the unique yolk-shell structure and synergistic effect between Mn and Co, the optimized Mn-Co-P catalysts exhibit outstanding performance toward both HER and OER. More importantly, a low cell voltage of 1.74 V is needed to achieve a current density of 10 mA cm^{-2} when Mn-Co-P is employed for overall water splitting. Our work not only establishes a yolk-shell structured Mn-Co-P as HER/OER bifunctional catalyst towards overall water splitting, but also provides a fabrication procedure that can be extended to other ternary transition metal phosphides.

4. Experimental Section

Materials synthesis: In a typical synthesis process, manganese acetate tetrahydrate (0.25 mmol, $Mn(CH_3COO)_2 \cdot 4H_2O$), cobalt nitrate hexahydrate (0.5 mmol, $Co(NO_3)_2 \cdot 6H_2O$) and urea (8 mmol) were dissolved in ethylene glycol (15 mL). After continuous magnetic stirring

for 30 min, the solution was transferred into a Teflon-lined stainless-steel autoclave and kept at 180 ℃ for 8 h. After cooling down to room temperature, the purple Mn-Co precursor powder was collected by centrifugation and then washed by deionized water and ethanol for several times, followed by being dried at 60 ℃. Finally, the precursor was annealed in a quartz furnace under flowing Ar with heating rate of 2 ℃ min^{-1} at 400 ℃ for 2 h to obtain the black Mn-Co-P products.

Material characterization: The morphologies were observed by scanning electron microscopy (SEM, ZEISS Sigma) and transmission electron microscopy (TEM, PEI Tecnai F30) equipped with energy dispersive spectrometer (EDS). Powder X-ray diffraction (XRD) patterns were recorded using a Rigaku X-ray diffractometer. X-ray photoelectron spectroscopy (XPS) was performed to investigate the chemical composition using a PHI Quantum-2000 spectrometer.

Electrochemical measurements: The electrocatalytic activity was evaluated with a typical three-electrode setup in 1 M KOH where a saturated calomel electrode (SCE) and a graphite electrode were used as the reference electrode and counter electrode, respectively. The Mn-Co-P power (2 mg) was dispersed in 100 εL solution containing deionized water (30 εL), ethanol (50 εL) and Nafion solution (0.5 wt.%, 20 εL), and then vibrated with ultrasonic for 10 min to get homogenous suspension. Afterwards, the homogenous suspension was coated onto conducting carbon paper (CP, 1 cm × 1 cm) and dried under ambient temperature. The catalyst loading amount is about 1.7 mg cm^{-2}. All the potentials were referred to a reversible hydrogen electrode (RHE) based on the conversion equation ($E_{RHE} = E_{SCE} + 0.0591 \times pH + 0.2415$).

Supporting Information

Supporting Information is available from the Wiley Online Library or from the author.

Acknowledgements

This research is financially supported by the National Nature Science Foundation of China (No. 51372212, 51601163).

WILEY-VCH

Received: ((will be filled in by the editorial staff))
Revised: ((will be filled in by the editorial staff))
Published online: ((will be filled in by the editorial staff))

References

[1] H. Zhao, Z. Y. Yuan, *Catal. Sci. Technol.* **2017**, *7*, 330-347.

[2] J. Q. Sun, S. E. Lowe, L. J. Zhang, Y. Z. Wang, K. L. Pang, Y. Wang, Y. L. Zhong, P. R. Liu, K. Zhao, Z. Y. Tang, H. J. Zhao, *Angew. Chem., Int. Ed.* **2018**, *57*, 16511-16515.

[3] Y. H. Zhu, Y. B. Yin, X. Yang, T. Sun, S. Wang, Y. S. Jiang, J. M. Yan, X. B. Zhang, *Angew. Chem., Int. Ed.* **2017**, *56*, 7881-7885.

[4] Y. H. Zhu, X. Yang, X. B. Zhang, *Angew. Chem., Int. Ed.* **2017**, *56*, 6378-6380.

[5] L. Wei, K. L. Goh, O. Birer, H. E. Karahan, J. Chang, S. L. Zhai, X. C. Chen, Y. Chen, *Nanoscale* **2017**, *9*, 4401-4408.

[6] X. Wang, L. Z. Zhuang, Y. Jia, H. L. Liu, X. C. Yan, L. Z. Zhang, D. J. Yang, Z. H. Zhu, X. D. Yao, *Angew. Chem., Int. Ed.* **2018**, *57*, 16421-16425.

[7] C. Z. Yang, O. Fontaine, J. M. Tarascon, A. Grimaud, *Angew. Chem., Int. Ed.* **2017**, *56*, 8652-8656.

[8] A. P. Wu, Y. Xie, H. Ma, C. G. Tian, Y. Gu, H. J. Yan, X. M. Zhang, G. Y. Yang, H. G. Fu, *Nano Energy* **2018**, *44*, 353-363.

[9] J. Y. Jiang, C. Y. Yan, X. H. Zhao, H. X. Luo, Z. M. Xue, T. C. Mu, *Green Chem.* **2017**, *19*, 3023-3031.

[10] H. Rahaman, K. Barman, S. Jasimuddin, S. K. Ghosh, *RSC Adv.* **2016**, *6*, 113694-113702.

[11] Q. Gao, C. Q. Huang, Y. M. Ju, M. R. Gao, J. W. Liu, D. An, C. H. Cui, Y. R. Zheng, W. X. Li, S. H. Yu, *Angew. Chem., Int. Ed.* **2017**, *56*, 7769-7773.

[12] I. Vassalini, L. Borgese, M. Mariz, S. Polizzi, G. Aquilanti, P. Ghigna, A. Sartorel, V. Amendola, I. Alessandri, *Angew. Chem., Int. Ed.* **2017**, *56*, 6589-6593.

[13] Z. H. Pu, I. S. Amiinu, Z. K. Kou, W. Q. Li, S. C. Mu, *Angew. Chem., Int. Ed.* **2017**, *56*, 11559-11564.

[14] H. S. Fan, H. Yu, Y. F. Zhang, Y. Zheng, Y. B. Luo, Z. F. Dai, B. Li, Y. Zong, Q. Y. Yan, *Angew. Chem., Int. Ed.* **2017**, *56*, 12566-12570.

[15] Y. Tong, P. Z. Chen, T. P. Zhou, K. Xu, W. S. Chu, C. Z. Wu, Y. Xie, *Angew. Chem., Int. Ed.* **2017**, *56*, 7121-7125.

[16] F. W. Ming, H. F. Liang, H. H. Shi, X. Xu, G. Mei, Z. C. Wang, *J. Mater. Chem. A* **2016**, *4*, 15148-15155.

[17] J. W. Huang, Y. R. Li, Y. F. Xia, J. T Zhu, Q. H. Yi, H. Wang, J. Xiong, Y. H. Sun, G. F. Zou, *Nano Res.* **2017**, *10*, 1010-1020.

[18] C. Dai, X. K. Tian, Y. L. Nie, C. Tian, C. Yang, Z. X. Zhou, Y. Li, X. Y Gao, *Chem. Eng. J.* **2017**, *321*, 105-112.

[19] H. F. Liang, H. H. Shi, D. F. Zhang, F. W. Ming, R. R. Wang, J. Q. Zhuo, Z. C. Wang, *Chem. Mater.* **2016**, *28*, 5587-5591.

[20] T. T. Liu, Y. H. Liang, Q. Liu, X. P. Sun, Y. Q. He, A. M. Asiri, *Electrochem. Commun.* **2015**, *60*, 92-96.

[21] X. L. Liu, Y. X. Yang, S. Y. Guan, *Chem. Phys. Lett.* **2017**, *675*, 11-14.

[22] S. Wei, X. X. Wang, J. M. Wang, X. P. Sun, L. Cui, W. R. Yang, Y. W. Zheng, J. Q. Liu, *Electrochim. Acta* **2017**, *246*, 776-782.

[23] J. Q. Tian, Q. Liu, A. M. Asiri, X. P. Sun, *J. Am. Chem. Soc.* **2014**, *136*, 7587-7590.

[24] J. Deng, D. H. Deng, X. H. Bao, *Adv. Mater.* **2017**, *29*, 1606967.

[25] Y. Rao, Y. Wang, H. Ning, P. Li, M. B. Wu, *ACS Appl. Mater. Interfaces* **2016**, *8*, 33601-33607.

[26] J. W. Li, W. M. Xu, J. X. Luo, D. Zhou, D. W. Zhang, L. C. Wei, P. M. Xu, D. S. Yuan, *Nano-Micro Lett.* **2017**, *10*, 6.

[27] L. Liu, Z. Q. Jiang, L. Fang, H. T. Xu, H. J. Zhang, X. Gu, Y. Wang, *ACS Appl. Mater. Interfaces* **2017**, *9*, 27736-27744.

[28] Y. Pan, K. A. Sun, S. J. Liu, X. Cao, K. L. Wu, W. C. Cheong, Z. Chen, Y. Wang, Y. Li, Y. Q. Liu, D. S. Wang, Q. Peng, C. Chen, Y. D. Li, *J. Am. Chem. Soc.* **2018**, *140*, 2610-2618.

[29] J. Y. Li, M. Yan, X. M. Zhou, Z. Q. Huang, Z. M. Xia, C. R. Chang, Y. Y. Ma, Y. Q. Qu, *Adv. Funct. Mater.* **2016**, *26*, 6785-6796.

[30] Q. S. Liang, K. K. Huang, X. F. Wu, X. Y. Wang, W. Ma, S. H. Feng, *RSC Adv.* **2017**, *7*, 7906-7913.

[31] W. J. Jiang, S. Niu, T. Tang, Q. H. Zhang, X. Z. Liu, Y. Zhang, Y. Y. Chen, J. H. Li, L. Gu, L. J. Wan, J. S. Hu, *Angew. Chem., Int. Ed.* **2017**, *56*, 6572-6577.

[32] L. Jiao, Y. X. Zhou, H. L. Jiang, *Chem. Sci.* **2016**, *7*, 1690-1695.

[33] J. H. Song, C. Z. Zhu, B. Z. Xu, S. F. Fu, M. H. Engelhard, R. F. Ye, D. Du, S. P. Beckman, Y. H. Lin, *Adv. Energy Mater.* **2017**, *7*, 1601555.

[34] K. L. Liu, F. M. Wang, T. A. Shifa, Z. X. Wang, K. Xu, Y. Zhang, Z. Z. Cheng, X. Y. Zhan, J. He, *Nanoscale* **2017**, *9*, 3995-4001.

[35] H. X. Zhang, Q. Ding, D. H. He, H. Liu, W. Liu, Z. J. Li, B. Yang, X. W. Zhang, L. C. Lei, S. Jin, *Energy Environ. Sci.* **2016**, *9*, 3113-3119.

[36] B. Y. Guan, L. Yu, X. W. Lou, *Angew. Chem., Int. Ed.* **2017**, *56*, 2386-2389.

[37] X. J. Hou, X. F. Wang, B. Liu, Q. F. Wang, T. Luo, D. Chen, G. Z. Shen, *Nanoscale* **2014**, *6*, 8858-8864.

[38] S. Natarajan, S. Anantharaj, R. J. Tayade, H. C. Bajaj, S. Kundu, *Dalton Trans.* **2017**, *46*, 14382-14392.

[39] Y. M. Dong, L. G. Kong, G. L. Wang, P. P. Jiang, N. Zhao, H. Z. Zhang, *Appl. Catal., B* **2017**, *211*, 245-251.

[40] J. F. Chang, Y. Xiao, M. L. Xiao, J. J. Ge, C. P. Liu, W. Xing, *ACS Catal.* **2015**, *5*, 6874-6878.

[41] H. F. Liang, F. Meng, M. Caban-Acevedo, L. S. Li, A. Forticaux, L. C. Xiu, Z. C. Wang, S. Jin, *Nano Lett.* **2015**, *15*, 1421-1427.

[42] L. Jiao, Y. X. Zhou, H. L. Jiang, *Chem. Sci.* **2016**, *7*, 1690-1695.

[43] J. Bao, J. F. Xie, F. C. Lei, Z. L. Wang, W. J. Liu, L. Xu, M. L. Guan, Y. Zhao, H. M. Li, *Catalysts* **2018**, *8*, 350.

[44] C. D. Bai, S. S. Wei, D. R. Deng, X. D. Lin, M. S. Zheng, Q. F. Dong, *J. Mater. Chem. A* **2017**, *5*, 9533-9536.

[45] G. Mei, H. F. Liang, B. B. Wei, H. H. Shi, F. W. Ming, X. Xu, Z. C. Wang, *Electrochim. Acta* **2018**, *290*, 82-89.

[46] S. R. Chen, M. L. Gordin, R. Yi, G. Howlett, H. Sohn, D. H. Wang, *Phys. Chem. Chem. Phys.* **2012**, *14*, 12741-12745.

[47] D. Li, H. Baydoun, C. N. Verani, S. L. Brock, *J. Am. Chem. Soc.* **2016**, *138*, 4006-4009.